Original Article

Engineering of an endogenous hydrogen sulfide responsive smart agent for photoacoustic imaging-guided combination of photothermal therapy and chemotherapy for colon cancer

Qiwei Tian [a,b], Xiaodong Wang [c], Shaoli Song [b,*], Lu An [c], Shiping Yang [c,*], Gang Huang [a,*]

[a] Shanghai Key Laboratory of Molecular Imaging, Jiading District Central Hospital Affiliated Shanghai University of Medicine and Health Sciences, Shanghai University of Medicine and Health Sciences, Shanghai 201318, China
[b] Department of Nuclear Medicine, Fudan University Shanghai Cancer Center, Shanghai, China
[c] Shanghai Municipal Education Committee Key Laboratory of Molecular Imaging Probes and Sensors, Shanghai Normal University, Shanghai 200234, China

HIGHLIGHTS

- Engineering of a endogenous hydrogen sulfide responsive combination of photothermal therapy and chemotherapy for colon cancer.
- HKUST-1 was loaded with curcumin as an endogenous hydrogen sulfide-triggered smart agent.
- Cur@HKUST-1@PVP allows selective colon cancer tumor imaging.

GRAPHICAL ABSTRACT

An endogenous hydrogen sulfide-responsive smart agent (Cur@HKUST-1@PVP) was engineered for a combination of photoacoustic imaging-guided PTT and chemotherapy for colon cancer.
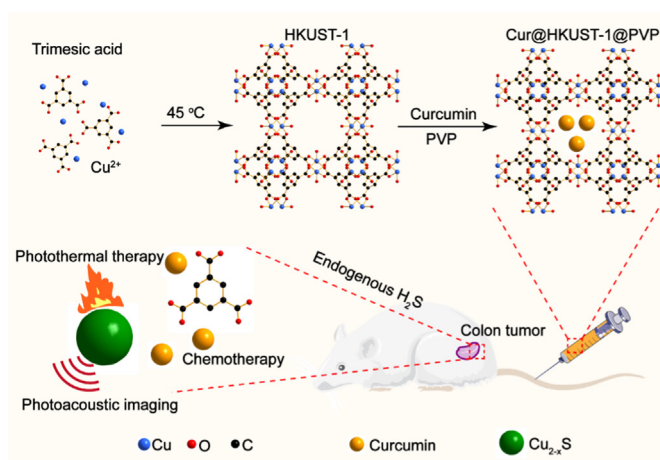
ARTICLE INFO

ABSTRACT

Introduction: Photothermal therapy can be synergistically combined with chemotherapy to improve the therapeutic effect for colon cancer. However, conventional therapeutic agents have side effects in normal tissues, limiting their application.
Objectives: To reduce these side effects, a smart agent (Cur@HKUST-1@PVP) whose functionality is triggered by the high content of endogenous hydrogen sulfide in colon tumors was engineered for photoacoustic imaging-guided combination of photothermal therapy and chemotherapy for colon tumors.
Methods: After reacting with hydrogen sulfide, Cur@HKUST-1@PVP simultaneously generates CuS and releases curcumin. The generated CuS serves as an imaging agent for both photothermal therapy and photoacoustic imaging, while the released curcumin is used for chemotherapy.

Smart agent
Colon cancer

Results: In vivo photoacoustic imaging experiments demonstrated that Cur@HKUST-1@PVP can be used for selectively imaging colon cancer tumors. In vivo experiments in mice for treatment suggested that the endogenous hydrogen sulfide-activated combination of photothermal therapy and chemotherapy has a better treatment effect that photothermal therapy or chemotherapy treatment alone.
Conclusion: The endogenous hydrogen sulfide-activated Cur@HKUST-1@PVP agent developed herein shows great potential for the accurate diagnosis and effective treatment of colon cancer.

Introduction

Colon cancer is the third most common cancer and the second leading cause of cancer-related deaths due to the limitations of traditional treatment methods such as surgery and chemotherapy [1,2]. Therefore, new and efficient treatment methods for colon tumors are urgently needed. Photothermal therapy (PTT) has recently emerged as a minimally invasive treatment method that is more efficient and less invasive compared to traditional treatment methods [3,4]. Hu's group demonstrated that cancer can be inhibited by PTT using CuS as the photothermal agent [5,6]. However, after intravenous administration, the CuS photothermal agent is non-specifically distributed, resulting in trauma to normal tissues in the path of light [7,8]. In addition, it is difficult for PTT alone to completely kill tumor cells due to the high expression of heat shock protein, leading to tumor recurrence [9,10]. To overcome these limitations of PTT, it is necessary to develop dual-functional smart agents for PTT whose functions are activated by the tumor microenvironment [11–14].

Chemotherapy is widely used in combination with PTT to enhance the treatment effect of PTT [15–17]. Chen's group demonstrated that the combination of chemotherapy and PTT based on a dual-functional agent (ultrasmall plasmonic gold nanorod vesicles loaded with reduced graphene oxide and doxorubicin) can effectively inhibit tumor growth [18]. However, doxorubicin is highly toxic to normal tissues [19,20]. Curcumin, a bioactive molecule derived from the spice turmeric, can prevent the development of colon cancer by shutting down the active form of cortical protein [21]. More importantly, curcumin has low toxicity and few side effects [22]. However, curcumin cannot be transported through the blood due to its hydrophobicity, which limits its clinical application [23,24]. Therefore, it is of great interest to engineer a smart curcumin-loaded PTT agent that can deliver the curcumin to tumor sites and whose PTT function is activated by the tumor microenvironment.

The high expression of endogenous hydrogen sulfide (0.3 to 3.4 mmolL^{-1}) is a unique characteristic of colon cancer tumors [25–27]. Thus, endogenous hydrogen sulfide has been widely used to trigger the function of theranostic agents [28–32]. Zhao and co-workers developed several endogenous hydrogen sulfide-activated PTT-based theranostic agents that exhibit enhanced theranostic effects for colon cancer [33]. Metal organic frameworks (MOFs) with relatively high porosity have been widely used as drug carriers due to their high drug-loading capacity [34,35]. More importantly, the MOFs are easily destroyed by the tumor microenvironment to release the loaded drugs [36,37]. For example, Xie and co-workers developed a tumor pH-activated, curcumin-loaded smart agent based on MIL-100 (a MOF based on trimesic acid and Fe) [38]. This agent achieved nearly complete tumor ablation. Based on these past results, engineering an endogenous hydrogen sulfide-responsive MOF with a high loading of curcumin has the potential to further enhance the treatment effect for colon cancer.

As a proof to concept, HKUST-1 (a MOF based on trimesic acid and Cu) was loaded with curcumin (Cur@HKUST-1@PVP) as an endogenous hydrogen sulfide-triggered smart agent for the treatment of colon cancer based on a combination of PTT and chemotherapy. As shown in Scheme 1, HKUST-1 was prepared according to a previous report [39]. Curcumin was then loaded into HKUST-1, with polyvinylpyrrolidone (PVP) serving as a surface ligand to block the release of curcumin. When Cur@HKUST-1@PVP is enriched at the tumor site via intravenous administration, the Cu^{2+} in HKUST-1 reacts with endogenous hydrogen sulfide in the colon cancer tumor microenvironment, destroying the framework of HKUST-1. Subsequently, the generated CuS serves as an agent for photoacoustic imaging and PTT, while the curcumin released from HKUST-1 can be used for chemotherapy. The hydrogen sulfide-triggered photoacoustic imaging and drug release along with the efficacy of the combination of PTT and chemotherapy were investigated both in vitro and in vivo. This work not only provides a new smart agent for colon cancer therapy, it also affords an engineering strategy for smart agents.

Results and discussion

Synthesis and characterization of Cur@HKUST-1@PVP

The crystal structure, morphology, and size of the obtained Cur@HKUST-1@PVP were characterized by X-ray diffraction (XRD), transmission electron microscopy (TEM), and dynamic light scattering (DLS), respectively. As shown in Fig. 1a, the diffraction patterns of the prepared HKUST-1, Cur@HKUST-1, and Cur@HKUST-1@PVP match well with the simulated HKUST-1 pattern. The characteristic peak of curcumin (C–O stretching vibration of aromatic hydrocarbons at 1285 cm^{-1}) and PVP (C = O bond vibrations at 1660 cm^{-1}) on Fourier transform infrared (FT-IR) spectroscopy demonstrates the existence of curcumin and PVP in the Cur@HKUST-1@PVP nanoparticles (Figure S1) [40,41]. Moreover, the crystal structure of Cur@HKUST-1@PVP is similar to those of HKUST-1 and Cur@HKUST-1, indicating that the HKUST-1 crystalline structure was not affected by the loading of curcumin and modification with PVP. According to the TEM analysis (Fig. 1b), Cur@HKUST-1@PVP exhibited a spherical shape with a particle size of approximately 110 nm, similar to the particle sizes of HKUST-1 and Cur@HKUST-1 (Figure S2). The DLS results further demonstrate that particle size of Cur@HKUST-1@PVP was approximately 110 nm, slightly larger than the sizes of HKUST-1 and Cur@HKUST-1 (Fig. 1c). The loading of curcumin was investigated by ultraviolet–visible (UV–VIS) spectroscopy (Figure S3). The absorption at 428 nm, corresponding the n–p* transition in curcumin, of Cur@HKUST-1@PVP further suggests the successful loading of curcumin (Figure S4) [42]. In addition, as the amount of added curcumin increased, the drug loading quickly increased and plateaued at approximately 0.5 mg/mg, which can be considered as the maximum curcumin loading of HKUST-1 (Fig. 1d). The above results demonstrate that the Cur@HKUST-1@PVP was successfully prepared and could be used in further experiments.

Hydrogen sulfide-responsive performance of Cur@HKUST-1@PVP

To investigate the hydrogen sulfide-responsive performance of Cur@HKUST-1@PVP, sodium hydrosulfide (NaHS) was used to
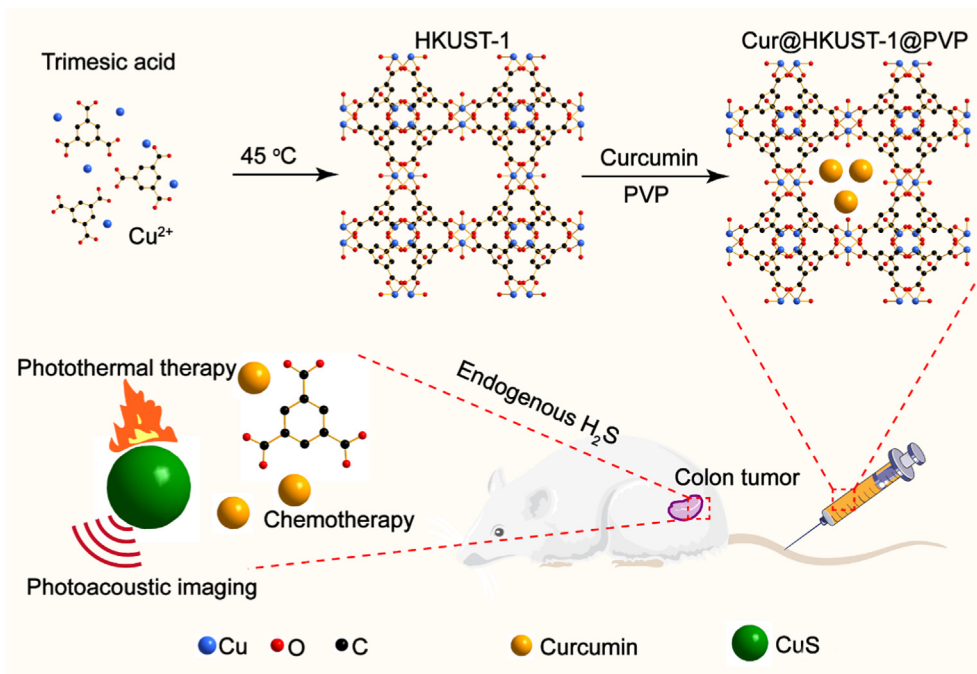
Scheme 1. Schematic showing the engineering of Cur@HKUST-1@PVP as an endogenous hydrogen sulfide-triggered smart agent for colon cancer therapy based on a combination of PTT and chemotherapy.
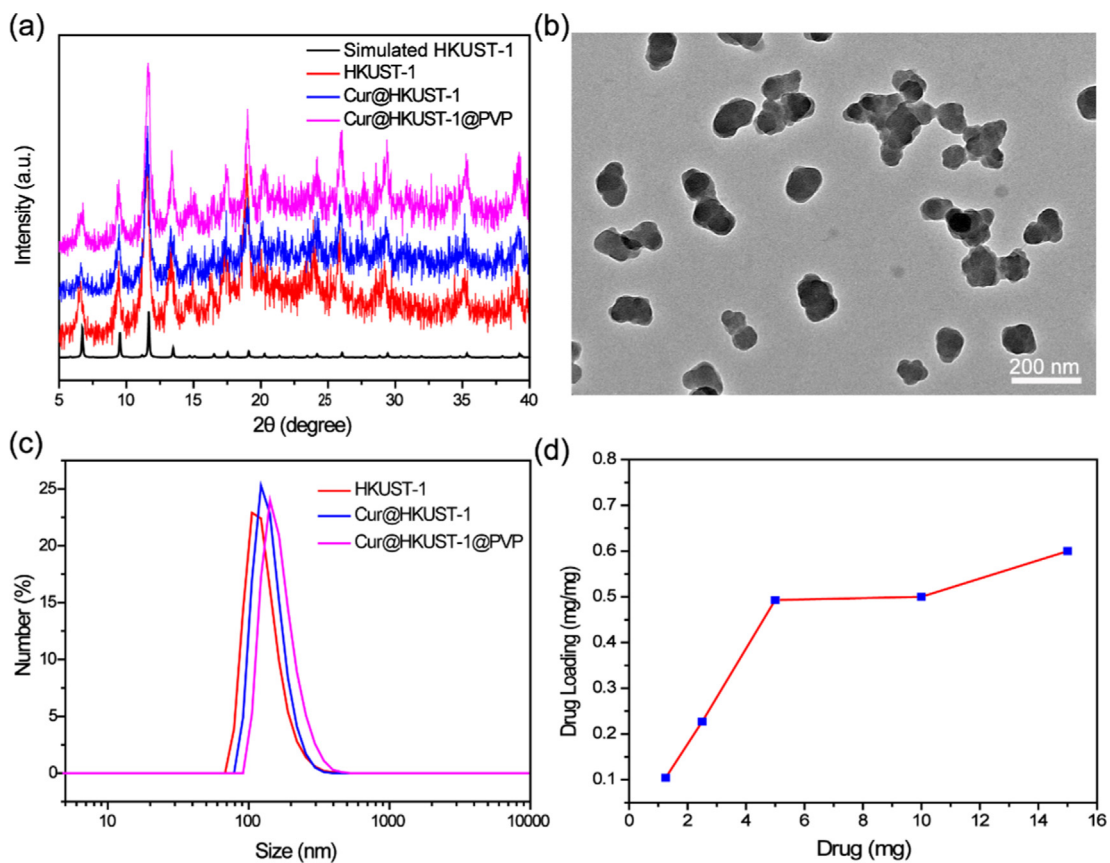

Fig. 1. (a) XRD patterns of HKUST-1 (red line), Cur@HKUST-1 (blue line), and Cur@HKUST-1@PVP (pink line) and the simulated pattern of HKUST-1 (black line). (b) TEM image of Cur@HKUST-1@PVP. (c) DLS spectra of HKUST-1 (red line), Cur@HKUST-1 (blue line), and Cur@HKUST-1@PVP (pink line). (d) Drug loading curve of HKUST-1 (curcumin loading amount vs. the amount of added curcumin).

simulate endogenous hydrogen sulfide. First, we investigated the change in crystal structure in the presence of NaHS. As shown in Fig. 2a, the XRD peak of Cur@HKUST-1@PVP after reaction with NaHS matched well with the peak of the covellite phase of CuS (JCPDS NO.1–1281), suggesting the generation of CuS. The generated CuS was in the form of nanospheres with sizes of approximately 15 nm (Fig. 2b), much smaller than the obtained Cur@HKUST-1@PVP (Figure S5). Subsequently, the effects of NaHS concentration, reaction time, pH (4–9), and common substances on the hydrogen sulfide-responsive performance were explored. The concentration of NaHS strongly affected the absorption of Cur@HKUST-1@PVP (Figure S6), especially in the near-infrared (NIR) region. As shown in Fig. 2c, the absorption of Cur@HKUST-1@PVP at 980 nm was very weak; the absorption intensity increased gradually as the amount of added NaHS increased from 0.5 to 3.5 mM but did not increase significantly when the concentration of NaHS increased beyond 3.5 mM (Fig. 2c). As the reaction time increased, the absorbance at 980 nm first increased rapidly and then increased more slowly when the reaction time reached 40 min (Fig. 2d and S7), indicating that the vulcanization reaction of Cur@HKUST-1@PVP was essentially completed in 40 min. Importantly, neither the pH (4, 5, 6, 6.5, 7, 8 and 9) nor the presence of common substances in organisms [Cl^-, CO_3^{2-}, SO_4^{2-}, OAc^-, HPO_4^{2-}, F^-, $S_2O_3^{2-}$, L-cysteine (L-Cys), serine (Ser), glycine (Gly), glutathione (GSH), and bovine serum albumin (BSA)] affected the change in absorption of Cur@HKUST-1@PVP obviously after reaction with NaHS (Fig. 2e and 2f). That the absorption change is unaffected by most of the interfering substance can be assigned to the stronger binding ability between Cu^{2+} in HKUST-1 and S^{2-} generated from NaHS. Whereas, the slightly absorption change for pH = 4, BSA et al. can be attributed that the acidity of such substances affects the generation of S^{2-} from NaHS. The XRD, TEM, and UV–VIS results all indicate that Cur@HKUST-1@PVP was triggered effectively by hydrogen sulfide to release curcumin and generate CuS with strong NIR absorption.

Hydrogen sulfide-triggered imaging and therapy performance

The strong NIR absorption of Cur@HKUST-1@PVP after reaction with NaHS inspired us to investigate its hydrogen sulfide-triggered photothermal and photoacoustic performance. First, thermal images of solutions containing different concentrations of Cur@HKUST-1@PVP and NaHS after 15 min of laser irradiation were collected to evaluate the photothermal performance of Cur@HKUST-1@PVP activated by NaHS. As shown in Fig. 3a and 3b, the thermal image color of the Cur@HKUST-1@PVP or NaHS solution (controls) hardly changed upon laser irradiation. In contrast, the colors of the thermal images of the mixtures of Cur@HKUST-1@PVP and NaHS changed from fiery red to luminous yellow as the concentration of Cur@HKUST-1@PVP or NaHS increased. Based on the quantitative analysis of the temperature change (ΔT), the ΔT of the Cur@HKUST-1@PVP solution was only 6 °C, while the ΔT for the mixture of 1 mM Cur@HKUST-1@PVP with 1–4 mM NaHS ranged from 10 °C to 21 °C. Similarly, the ΔT of the NaHS solution was 6 °C, while that for the mixture of 3 mM NaHS with 0.2–1 mM Cur@HKUST-1@PVP was 9 °C–19 °C. The obtained photothermal conversion efficiency of Cur@HKUST-1@PVP (1 mM) after activation by NaHS (3 mM) was calculated as 38.3% according to a previously reported method [6] (Figure S8), further demonstrating the good photothermal performance. After six cycles of laser irradiation (15 min on and 10 min off), the ΔT of the mixture of 3 mM NaHS with 0.6 mM Cur@HKUST-1@PVP exhibited no obvious change (Fig. 3c), indicating the good photothermal stability of activated Cur@HKUST-1@PVP.

The good photothermal performance of activated Cur@HKUST-1@PVP encouraged us to further investigated its photoacoustic imaging performance, which is closely related to the photothermal performance. As shown in Fig. 3d, the red color of the photoacoustic image of the Cur@HKUST-1@PVP dispersion without NaHS (control) changed to red as the concentration of NaHS increased from 0.5 to 4 mM. When the concentration of NaHS was 4 mM,
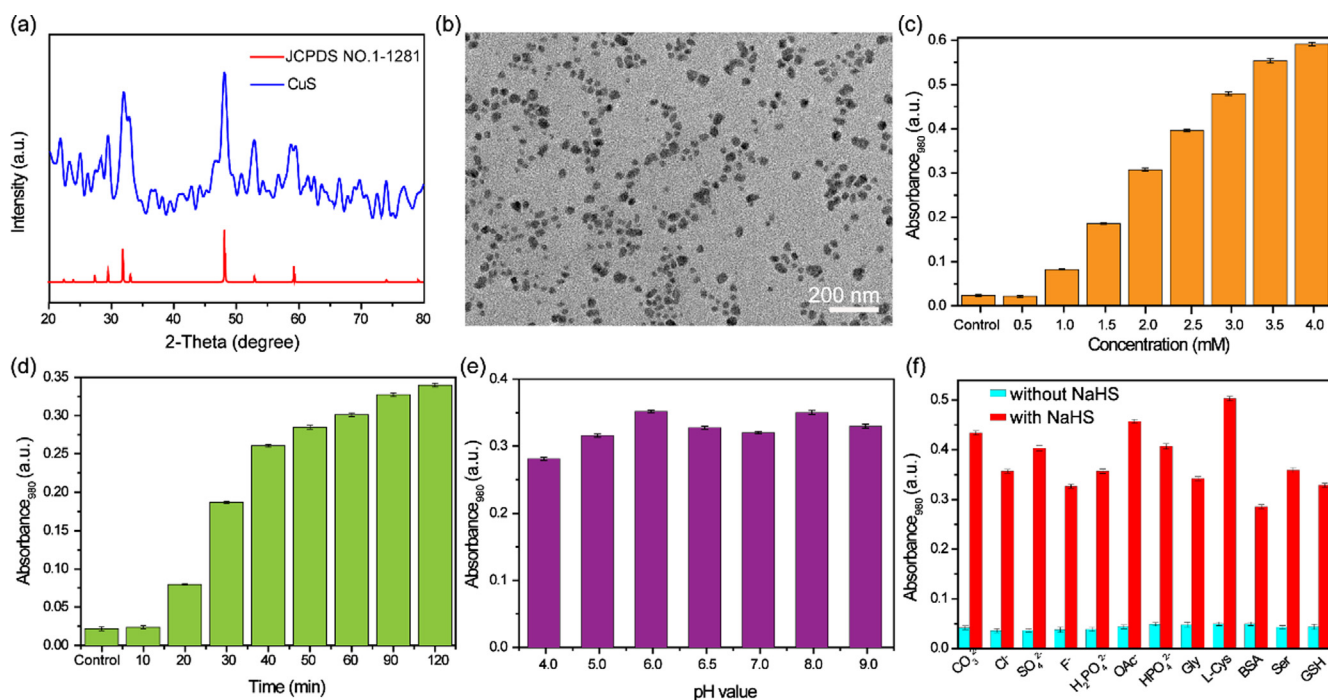

Fig. 2. (a) XRD patterns of the CuS generated by the reaction of Cur@HKUST-1@PVP with NaHS (blue line) and the covellite phase of CuS (red line). (b) TEM image of the CuS generated by the reaction of Cur@HKUST-1@PVP with NaHS. (c) Absorbance at 980 nm of Cur@HKUST-1@PVP before (control) and after reaction with different concentrations of NaHS (0.5–4.0 mM). (d) Absorbance at 980 nm of Cur@HKUST-1@PVP before (control) and after reaction with NaHS for different times (10–120 min). (e) Absorbance at 980 nm of Cur@HKUST-1@PVP after reaction with NaHS at different pH values. (f) Absorbance at 980 nm of Cur@HKUST-1@PVP before and after reaction with NaHS in the presence of different common substances.
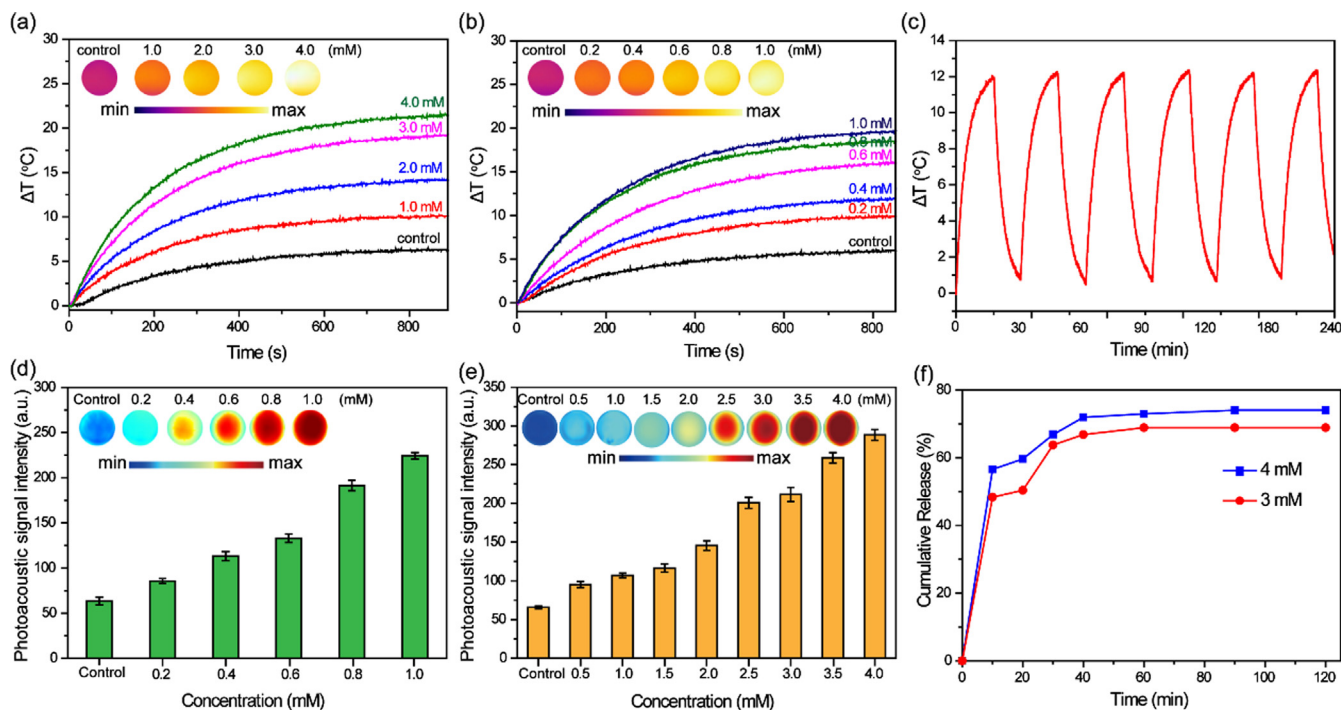
Fig. 3. (a) Thermal images (inset) and corresponding plots of ΔT vs. time for Cur@HKUST-1@PVP before (control) and after reaction with different concentrations of NaHS (1–4 mM). (b) Thermal images (inset) and corresponding plots of ΔT vs. time for NaHS before (control) and after reaction with different concentrations of Cur@HKUST-1@PVP (0.2–1 mM). (c) Photothermal stability of Cur@HKUST-1@PVP after reaction with NaHS. (d) Photoacoustic images and corresponding signal intensity of NaHS before (control) and after reaction with different concentrations of Cur@HKUST-1@PVP (0.2–1 mM). (e) Photoacoustic images and corresponding signal intensity of Cur@HKUST-1@PVP before (control) and after reaction with different concentrations of NaHS (0.5–4 mM). (f) Plots of curcumin release vs. time for the reaction of Cur@HKUST-1@PVP with 3 mM (red) and 4 mM (blue) NaHS.

the photoacoustic intensity was five times higher than that of the control. A similar photoacoustic effect was observed when the concentration of NaHS was fixed while the concentration of Cur@HKUST-1@PVP was altered (Fig. 3e). The photoacoustic imaging performance of Cur@HKUST-1@PVP was not affected by pH or the presence of various common substances (Figure S9). Considering the destruction of the crystal structure of Cur@HKUST-1@PVP upon the addition of NaHS, the curcumin release performance was explored based on the standard curve of concentration and absorption of curcumin (Figure S3). As shown in Fig. 3f, nearly 50% of curcumin was released from Cur@HKUST-1@PVP within 10 min after the addition of NaHS, and no obvious additional curcumin release occurred in the following 1 h. Thus, curcumin was released quickly from Cur@HKUST-1@PVP upon its reaction with NaHS. No obvious difference in release performance was observed after activation by 3 and 4 mM NaHS, further indicating that the crystal structure of Cur@HKUST-1@PVP was destroyed quickly by NaHS to release curcumin. The above results demonstrate that Cur@HKUST-1@PVP can be activated by NaHS for use in photoacoustic imaging as well as combined PTT and chemotherapy treatment.

Photoacoustic imaging of tumors

The good photoacoustic imaging performance of Cur@HKUST-1@PVP after activation by NaHS inspired us to further explore its photoacoustic imaging performance in a colon tumor-bearing mouse model in which endogenous hydrogen sulfide is highly expressed. As shown in Fig. 4a, the photoacoustic imaging color at the tumor site (marked by a green ellipse) was greatly different from that at the muscle site (marked by an orange ellipse) before (control) and after (0.5–1 h) the intratumoral injection of Cur@HKUST-1@PVP. The photoacoustic signal intensity at the

tumor site increased by approximately two times after the injection of Cur@HKUST-1@PVP, whereas that at the muscle site only increased by 0.4 times (Fig. 4b). The results demonstrate that the photoacoustic imaging function of Cur@HKUST-1@PVP was effectively activated by endogenous hydrogen sulfide in colon cancer tumors. Next, Cur@HKUST-1@PVP was investigated for colon tumor imaging. As shown in Fig. 4c, after the intravenous administration of Cur@HKUST-1@PVP, the photoacoustic imaging color at the tumor site over time was greatly different compared to that in the control group, with the color difference being greatest at 2 h after injection. The change in photoacoustic intensity at the tumor site after the injection of Cur@HKUST-1@PVP further demonstrated the imaging selectivity for colon cancer tumors. As shown in Fig. 4d, the signal at the tumor site was significantly enhanced upon the injection of Cur@HKUST-1@PVP, and the signal reached the maximum value at 2 h after injection; this maximum signal was approximately five times that at the tumor site before injection (control). The photoacoustic imaging results demonstrate that Cur@HKUST-1@PVP can be used for selective colon cancer tumor imaging.

Combined PTT and chemotherapy for the treatment of colon tumors

Considering the good biocompatibility (Figure S10), photothermal and curcumin release performances of Cur@HKUST-1@PVP, its applicability in combined PTT and chemotherapy for colon tumors was investigated in a colon tumor-bearing mouse model under the guidance of photoacoustic imaging. The colon tumor-bearing mice were randomly divided into four groups (control, curcumin, HKUST-1, and Cur@HKUST-1@PVP) and were intravenously administered with phosphate buffered saline (PBS), curcumin, HKUST-1, and Cur@HKUST-1@PVP, respectively. According to the photoacoustic imaging results, among the groups and times after
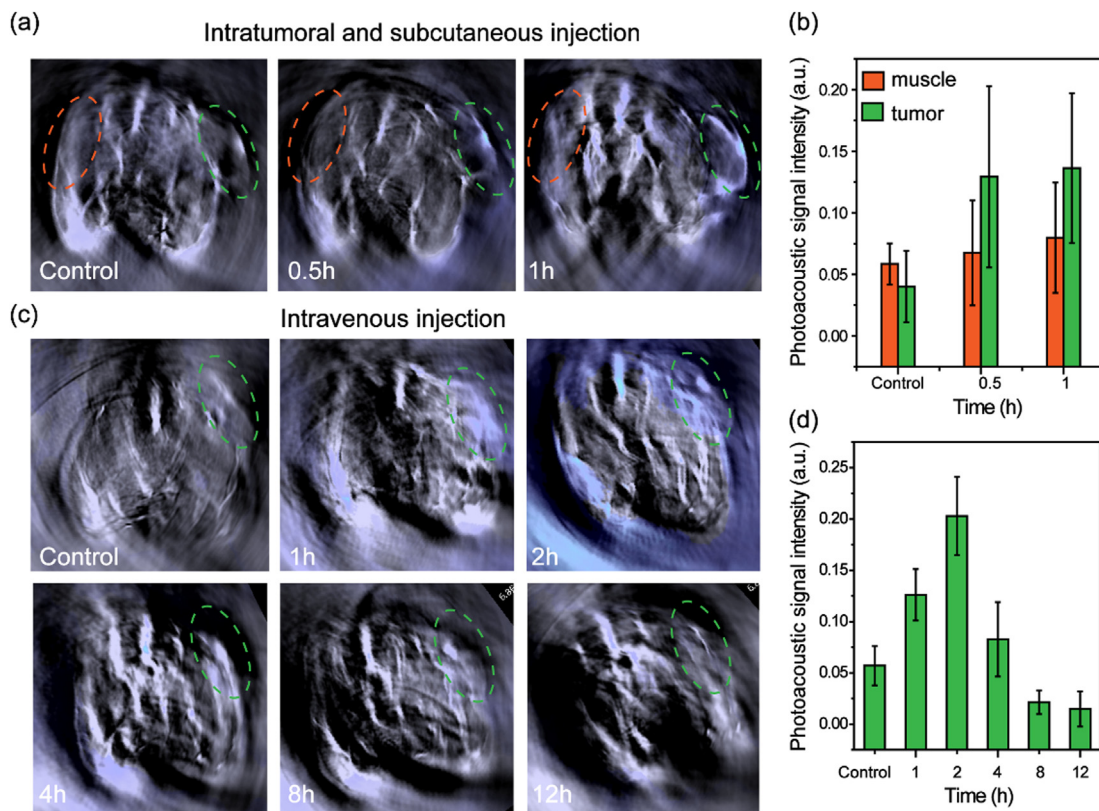
Fig. 4. (a) Photoacoustic images and (b) corresponding signal intensity of a colon tumor-bearing mouse before (control) and after the intratumoral and subcutaneous injection of Cur@HKUST-1@PVP at the tumor site (green ellipse) and muscle site (orange ellipse). (c) Photoacoustic images and (d) corresponding signal intensity of a colon tumor-bearing mouse model before (control) and at different times (1–12 h) after the intravenous administration of Cur@HKUST-1@PVP.

injection, the photoacoustic signal was the strongest in the Cur@HKUST-1@PVP group at 2 h after injection. Thus, compared to PBS, curcumin, and HKUST-1, Cur@HKUST-1@PVP was more enriched in the tumor. Therefore, PTT was carried out at 2 h after injection, and a thermal imaging camera was used to monitor the temperature change in the tumor during treatment. Among the four groups, the color change at the tumor site after 5 min of laser radiation was largest in the Cur@HKUST-1@PVP group (Fig. 5a). According to the plots of maximum temperature vs. time (Fig. 5b), the temperature increased from 30 °C to 36.2 °C, 38.8 °C, 42.6 °C, and 46.6 °C in the control, curcumin, HKUST-1, and Cur@HKUST-1@PVP groups, respectively. The highest temperatures observed in the Cur@HKUST-1@PVP groups after laser irradiation demonstrate that the endogenous hydrogen sulfide in the colon tumor microenvironment reacted with HKUST-1 to activate its PTT function.

To investigate the treatment effect, one mouse was randomly selected from each group at 4 h after treatment for the histological analysis of the tumors. As shown in Fig. 5c, the hematoxylin and eosin (H&E)-stained images of the tumor tissues from the control, curcumin, and HKUST-1 groups did not show obvious features of thermal necrosis. In contrast, the cells in the Cur@HKUST-1@PVP group showed characteristics of thermal necrosis, including incomplete cell outlines and the separation of nucleus and cytoplasm. This is because the temperature at the tumor site in the Cur@HKUST-1@PVP group under laser irradiation exceeded 42 °C, which is the temperature at which tumor cells begin to be killed according to a previous report [43]. The terminal deoxynucleotidyl transferase dUTP nick end labeling (TUNEL)-stained images of tumor tissues in the cur-

cumin, HKUST-1, and Cur@HKUST-1@PVP groups clearly showed apoptotic cells, in contrast to the tumor tissue from the control group. The quantitative analysis of the histological results further supported the findings from the H&E and TUNEL staining images (Figure S11). These results suggest that both chemotherapy (curcumin group) and PTT (HKUST-1) caused cell apoptosis, and the combination of the two (Cur@HKUST-1@PVP) better promoted apoptosis than either treatment alone. The above results demonstrate that Cur@HKUST-1@PVP can be used to treat colon tumors based on the endogenous hydrogen sulfide-activated combination of PTT and chemotherapy.

To further evaluate the effect of the combination of PTT and chemotherapy, the mice in each group were continuously monitored for 16 d after treatment. According to the collected images (Fig. 6a), the tumors grew quickly over 16 d in the control group. Compared to the control, tumor growth was significantly suppressed in both the curcumin and HKUST-1 groups, and the tumor disappeared completely in the Cur@HKUST-1@PVP group (Figure S12). The relative tumor volume (Fig. 6b), which was measured every day, further demonstrated that chemotherapy (curcumin group) or PTT (HKUST-1) alone could only suppress tumor growth to a certain extent; in contrast, the combination of PTT and chemotherapy (Cur@HKUST-1@PVP) could completely eliminate the tumor. The body weights of the mice in the four groups did not change significantly during the observation period (Fig. 6c), suggesting the good biocompatibility of the treatment agents. These results demonstrate that after triggering by endogenous hydrogen sulfide, Cur@HKUST-1@PVP can not only achieve selective colon tumor imaging, it can also cure tumors based on a combination of PTT and chemotherapy.
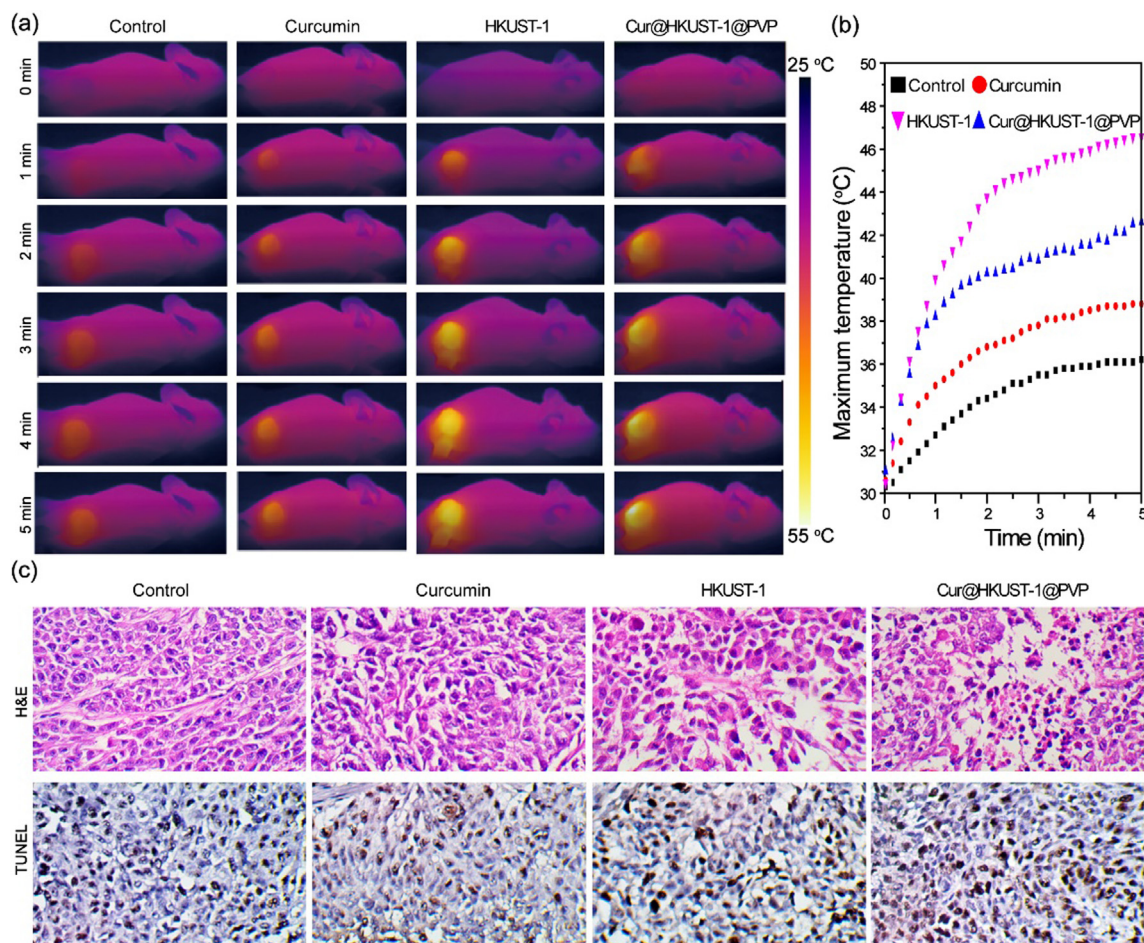
Fig. 5. (a) Photothermal images and (b) corresponding plots of maximum temperature vs. time in colon tumor-bearing mice under laser irradiation after the intravenous administration of PBS, curcumin, HKUST-1, and Cur@HKUST-1@PVP. (c) Histological analysis of tumors from mice in different groups stained by H&E (upper panel) and TUNEL (lower panel).

Conclusion

In summary, Cur@HKUST-1@PVP, an endogenous hydrogen sulfide-responsive smart agent, was successfully engineered for a combination of photoacoustic imaging-guided PTT and chemotherapy for colon cancer. After reacting with hydrogen sulfide, Cur@HKUST-1@PVP simultaneously generates CuS and releases curcumin. The generated CuS serves as both photothermal and photoacoustic imaging agents, while the released curcumin is effective for chemotherapy. In vivo photoacoustic imaging experiments demonstrated that Cur@HKUST-1@PVP allows selective colon cancer tumor imaging. Based on in vivo treatment experiments using a colon tumor-bearing mouse model, the combination of PTT and chemotherapy activated by endogenous hydrogen sulfide using Cur@HKUST-1@PVP has a better treatment effect than either single treatment alone. The endogenous hydrogen sulfide-activated Cur@HKUST-1@PVP shows great potential for the accurate diagnosis and effective treatment of colon cancer.

Experimental

Chemicals and materials

Cupric acetate, trimesic acid, and curcumin were purchased from Sinopharm Chemical Reagent (Shanghai, China). PVP (MW = 29000) and NaHS were purchased from Sigma-Aldrich.

Ethanol was bought from the exploration platform of Shanghai Titan Technology Co., Ltd (Shanghai, China). All reagents were used without further purification.

Synthesis of Cur@HKUST-1@PVP

First, HKUST-1 was prepared following the previous report [39]. Next, curcumin was loaded into HKUST-1 via a co-incubation method in which equal amounts of the curcumin and HKUST-1 were incubated in ethanol for 12 h at 37 °C. Excess curcumin was removed by centrifugation. Subsequently, to prevent the release of loaded curcumin, Cur@HKUST-1 was modified with PVP by adding 2 mg PVP into a 10-mL solution of Cur@HKUST-1 (1 mM) in ethanol under stirring for 30 min at room temperature. Cur@HKUST-1@PVP was purified by centrifugation and washing two times with ethanol.

Characterization

The morphologies of the prepared materials were observed by scanning electron microscopy (SEM; Zeiss, EVO MA 25/LS 25) and TEM (JEOL 2011F). The crystal structure was confirmed by powder XRD (Rigaku DMAX2000). DLS (Malvern Nano-ZS90) was used to identify the diameters of the obtained nanoparticles. A Beckman Coulter DU 730 UV–VIS-NIR spectrophotometer was used to measure the absorptions of obtained nanoparticles.
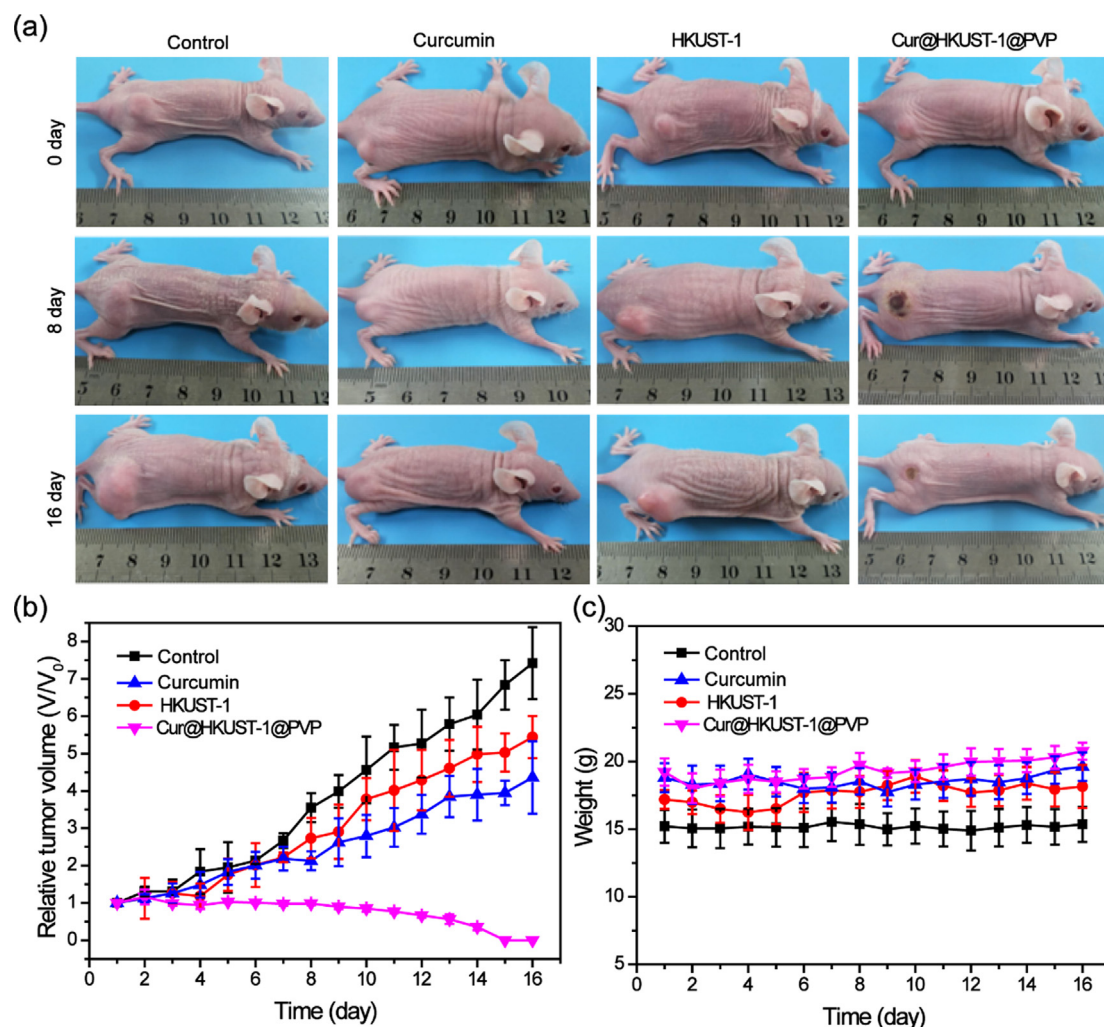
Fig. 6. (a) Photographs of the colon tumor-bearing mice at 1 d before and at 8 and 16 d after the injection of PBS (control), curcumin, HKUST-1, and Cur@HKUST-1@PVP. (b) Relative tumor volumes and (c) body weights of the colon tumor-bearing mice at 1–16 days after injection with PBS (control), curcumin, HKUST-1, and Cur@HKUST-1@PVP.

Hydrogen sulfide-responsive performance

NaHS was used to simulate endogenous hydrogen sulfide to explore the response performance of Cur@HKUST-1@PVP in solution. To confirm the reaction between NaHS and Cur@HKUST-1@PVP, an equal volume of NaHS (4 mM) and Cur@HKUST-1@PVP (1 mM) were mixed and incubated for 2 h at room temperature. The generated nanoparticles were collected by centrifugation and characterized by TEM and XRD.

To explore the effect of the NaHS concentration on the absorption of Cur@HKUST-1@PVP, equal volumes of NaHS (0.5, 1, 1.5, 2, 2.5, 3, 3.5, or 4 mM) and Cur@HKUST-1@PVP (1 mM) were mixed, and the absorption of each mixture was measured after 1 h at room temperature. A dispersion of Cur@HKUST-1@PVP (1 mM) alone was used as the control.

To investigate the effect of reaction time on Cur@HKUST-1@PVP absorption, equal volumes of NaHS (3 mM) and Cur@HKUST-1@PVP (1 mM) were mixed and allowed to react for different times. The absorption of the mixture was measured before mixing with NaHS (control) and after 10, 20, 30, 40, 50, 60, 90, and 120 min after adding NaHS.

To study the effect of pH on Cur@HKUST-1@PVP absorption, NaHS (3 mM) was added into equal volumes of Cur@HKUST-1@PVP (1 mM) dispersion with different pH values (4, 5, 6, 6.5, 7,

8, and 9). After 1 h of incubation, the absorption of the mixture was measured.

To evaluate the effects of common substrates on Cur@HKUST-1@PVP absorption after reacting with NaHS, Cur@HKUST-1@PVP (1 mM) was mixed with various common substrates (Cl^-, CO_3^{2-}, SO_4^{2-}, OAc^-, HPO_4^{2-}, F^-, $S_2O_3^{2-}$, L-Cys, serine, glycine, glutathione, and BSA; concentration = 3 mM). Next, an equal volume of NaHS (3 mM) was added into each mixture. After incubating for 1 h, the absorption of the mixture was measured.

Hydrogen sulfide-triggered photothermal performance and photoacoustic imaging

To explore the effect of NaHS concentration on the photothermal performance, equal volumes of NaHS (0.5, 1, 1.5, 2, 2.5, 3, 3.5, or 4 mM) and Cur@HKUST-1@PVP (1 mM) were mixed; a dispersion of Cur@HKUST-1@PVP (1 mM) alone was used as the control. To explore the effect of Cur@HKUST-1@PVP concentration on photothermal performance, equal volumes of Cur@HKUST-1@PVP (0.2, 0.4, 0.6, 0.8, or 1 mM) and NaHS (3 mM) were mixed; a solution of NaHS (3 mM) alone was used as the control. After reacting for 1 h at room temperature, a thermal camera (FLIR A310) was used to monitor the temperature changes of the mixtures under irradiation with a 980-nm laser at a power density of 0.5 W/cm^2

for 15 min. In addition, photoacoustic images of the mixtures were collected using a multispectral optoacoustic tomography imaging system (MSOT in Vision 128). To explore the photothermal stability of activated Cur@HKUST-1@PVP, equal volumes of NaHS (3 mM) and Cur@HKUST-1@PVP (0.6 mM) were mixed and subjected to six cycles of laser irradiation. Each cycle consisted of 15 min of laser on followed by 10 min of laser off.

Drug loading and release

To calculate the drug loading capacity, 10 mg of HKUST-1 (X) was incubated with 1, 2.5, 5, 10 or 20 mg of curcumin (Y) in ethanol for 12 h at 37 °C. Subsequently, the upper liquid containing excess curcumin was collected by centrifugation. The precipitate was then washed three times with ethanol and again separated by centrifugation to collect the upper liquid. Finally, the absorbance at 425 nm was measured after combining all the collected upper liquids to calculate the curcumin content in the supernatant (Y_s) according to the standard curve. The drug loading was calculated as $(Y - Y_s) / X$.

To investigate the hydrogen sulfide-triggered drug release, equal volumes of an NaHS dispersion in ethanol (3 or 4 mM) and Cur@HKUST-1@PVP (1 mM) containing α g of curcumin were mixed. After reacting for 2 h at 37 °C, the released curcumin in ethanol was collected using an ultrafiltration tube with a 10-kDa molecular weight cutoff. The absorbance at 425 nm was measured after combining all the collected curcumin ethanol solutions to calculate the amount of released curcumin (β) according to the standard curve. The drug release was calculated as β / α.

Ethics statement

Female BALB/C nude mice aged 4–6 weeks were purchased from the Shanghai Laboratory Animal Center. The storage and use of animals were guided by the Animal Ethics Committee of Shanghai University of Medicine and Health Sciences according the relevant laws and institutional guidelines (Approval no.2021-GZR-18).

Tumor model

To prepare the colon tumor-bearing mouse model, approximately 1×10^6 HCT116 tumor cells suspended in PBS were injected subcutaneously into the upper surface of the right hind limb of the nude mice. When the tumor size reached approximately 100 mm^3, the animals were used for in vivo photoacoustic imaging and tumor treatment.

Photoacoustic imaging in vivo

First, photoacoustic images of HCT116 tumor-bearing mice were collected before the intravenous administration of Cur@HKUST-1@PVP as a control to explore the photoacoustic imaging performance of Cur@HKUST-1@PVP for colon tumors. Next, the mice were intravenously administered with Cur@HKUST-1@PVP (10 mg/kg), and photoacoustic images were collected at 0.5, 1, 2, 4, 8, and 12 h after injection.

In vivo combination therapy

The HCT116 tumor-bearing mice were randomly divided into four groups with six mice in each group. The mice in the control, curcumin, HKUST-1, and Cur@HKUST-1@PVP groups were intravenously administered with PBS, curcumin solution, a dispersion of HKUST-1 in PBS, and a dispersion of Cur@HKUST-1@PVP in PBS (dosage = 10 mg/kg), respectively. At 2 h after injection, the mice in each group were irradiated with a 980-nm laser at a power density of 0.5 W/cm^2 for 5 min. During the irradiation period, the temperature change at the tumor site was monitored using a thermal camera (FLIR A310). After 4 h of laser irradiation, one mouse in each group was sacrificed for histological analysis by H&E and TUNEL staining. In addition, pictures, tumor volumes, and body weights were collected from the other mice in each group each day for 16 days after injection.

Compliance with Ethics Requirements

All Institutional and National Guidelines for the care and use of animals (fisheries) were followed.

Declaration of Competing Interest

The authors declare that they have no known competing financial interests or personal relationships that could have appeared to influence the work reported in this paper.

Appendix A. Supplementary material

Supplementary data to this article can be found online at https://doi.org/10.1016/j.jare.2022.01.018.

References

[1] Siegel RL, Miller KD, Goding Sauer A, Fedewa SA, Butterly LF, Anderson JC, et al. Colorectal cancer statistics, 2020. CA A Cancer J Clin 2020;70(3):145–64.

[2] Zhang Y, Chen Z, Li J. The current status of treatment for colorectal cancer in China: A systematic review. Medicine (Baltimore) 2017;96(40):e8242. doi: https://doi.org/10.1097/MD.0000000000008242.

[3] Jung HS, Verwilst P, Sharma A, Shin J, Sessler JL, Kim JS. Organic molecule-based photothermal agents: an expanding photothermal therapy universe. Chem. Soc. Rev. 2018;47(7):2280–97.

[4] Cheng L, Wang C, Feng L, Yang K, Liu Z. Functional Nanomaterials for Phototherapies of Cancer. Chem Rev 2014;114(21):10869–939.

[5] Huang X, Zhang W, Guan G, Song G, Zou R, Hu J. Design and Functionalization of the NIR-Responsive Photothermal Semiconductor Nanomaterials for Cancer Theranostics. Acc Chem Res 2017;50(10):2529–38.

[6] Tian Q, Jiang F, Zou R, Liu Q, Chen Z, Zhu M, et al. Hydrophilic Cu 9 S 5 Nanocrystals: A Photothermal Agent with a 25.7% Heat Conversion Efficiency for Photothermal Ablation of Cancer Cells in Vivo. ACS Nano 2011;5 (12):9761–71.

[7] Zhou M, Li J, Liang Su, Sood AK, Liang D, Li C. CuS Nanodots with Ultrahigh Efficient Renal Clearance for Positron Emission Tomography Imaging and Image-Guided Photothermal Therapy. ACS Nano 2015;9(7):7085–96.

[8] Liu X, Fu F, Xu K, Zou R, Yang J, Wang Q, et al. Folic acid-conjugated hollow mesoporous silica/CuS nanocomposites as a difunctional nanoplatform for targeted chemo-photothermal therapy of cancer cells. J Mater Chem B 2014;2 (33):5358. doi: https://doi.org/10.1039/C4TB00919C.

[9] Wang S, Tian Y, Tian W, Sun J, Zhao S, Liu Y, et al. Selectively Sensitizing Malignant Cells to Photothermal Therapy Using a CD44-Targeting Heat Shock Protein 72 Depletion Nanosystem. ACS Nano 2016;10(9):8578–90.

[10] Liu Y, Xu M, Zhao Y, Chen Xu, Zhu X, Wei C, et al. Flower-like gold nanoparticles for enhanced photothermal anticancer therapy by the delivery of pooled siRNA to inhibit heat shock stress response. J Mater Chem B 2019;7 (4):586–97.

[11] He T, Yuan Y, Jiang C, Blum NT, He J, Huang P, et al. Nicholas Thomas Blum, Jin He, Peng Huang, Jing Lin, Light-Triggered Transformable Ferrous Ion Delivery System for Photothermal Primed Chemodynamic Therapy. Angew Chem Int Ed 2021;60(11):6047–54.

[12] He T, He J, Younis MR, Blum NT, Lei S, Zhang Y, et al. Muhammad Rizwan Younis, Nicholas Thomas Blum, Shan Lei, Yinling Zhang, Peng Huang, Jing Lin, Dual-Stimuli-Responsive Nanotheranostics for Dual-Targeting Photothermal-Enhanced Chemotherapy of Tumor. ACS Appl Mater Interfaces 2021;13 (19):22204–12.

[13] Zhao H, Wang J, Li Xi, Li Y, Li C, Wang X, et al. A biocompatible theranostic agent based on stable bismuth nanoparticles for X-ray computed tomography/magnetic resonance imaging-guided enhanced chemo/photothermal/chemodynamic therapy for tumours. J Colloid Interface Sci 2021;604:80–90.

[14] Guan S, Liu X, Fu Y, Li C, Wang J, Mei Q, et al. A biodegradable "Nano-donut" for magnetic resonance imaging and enhanced chemo/photothermal/chemodynamic therapy through responsive catalysis in tumor microenvironment. J Colloid Interface Sci 2022;608:344–54.

[15] Park H, Yang J, Lee J, Haam S, Choi I-H, Yoo K-H. Multifunctional Nanoparticles for Combined Doxorubicin and Photothermal Treatments. ACS Nano 2009;3 (10):2919–26.

[16] Chen Q, Liang C, Wang C, Liu Z. An Imagable and Photothermal "Abraxane-Like" Nanodrug for Combination Cancer Therapy to Treat Subcutaneous and Metastatic Breast Tumors. Adv Mater 2015;27(5):903–10.

[17] Sun X, Wang C, Gao M, Hu A, Liu Z. Remotely Controlled Red Blood Cell Carriers for Cancer Targeting and Near-Infrared Light-Triggered Drug Release in Combined Photothermal-Chemotherapy. Adv Funct Mater 2015;25 (16):2386–94.

[18] Song J, Yang X, Jacobson O, Lin L, Huang P, Niu G, et al. Sequential Drug Release and Enhanced Photothermal and Photoacoustic Effect of Hybrid Reduced Graphene Oxide-Loaded Ultrasmall Gold Nanorod Vesicles for Cancer Therapy. ACS Nano 2015;9(9):9199–209.

[19] Yemm KE, Alwan LM, Malik AB, Salazar LG. Yemm, Laura M Alwan, A Bilal Malik, Lupe G Salazar, Renal toxicity with liposomal doxorubicin in metastatic breast cancer. J Oncol Pharm Pract 2019;25(7):1738–42.

[20] Kaminskas LM, McLeod VM, Kelly BD, Sberna G, Boyd BJ, Williamson M, et al. A comparison of changes to doxorubicin pharmacokinetics, antitumor activity, and toxicity mediated by PEGylated dendrimer and PEGylated liposome drug delivery systems. Nanomed Nanotechnol Biol Med 2012;8(1):103–11.

[21] Radhakrishnan VM, Kojs P, Young G, Ramalingam R, Jagadish B, Mash EA, et al. pTyr421 cortactin is overexpressed in colon cancer and is dephosphorylated by curcumin: involvement of non-receptor type 1 protein tyrosine phosphatase (PTPN1). PLoS ONE 2014;9(1):e85796. doi: https://doi.org/10.1371/journal.pone.0085796.

[22] Gou MaLing, Men Ke, Shi HuaShan, Xiang MingLi, Zhang J, Song J, et al. Curcumin-loaded biodegradable polymeric micelles for colon cancer therapy in vitro and in vivo. Nanoscale 2011;3(4):1558. doi: https://doi.org/10.1039/c0nr00758g.

[23] Liu Y, Chen F, Zhang K, Wang Q, Chen Y, Luo X. pH-Responsive reversibly cross-linked micelles by phenol–yne click via curcumin as a drug delivery system in cancer chemotherapy. J Mater Chem B 2019;7(24):3884–93.

[24] Sabra R, Billa N, Roberts CJ. An augmented delivery of the anticancer agent, curcumin, to the colon. React Funct Polym 2018;123:54–60.

[25] Papapetropoulos A, Pyriochou A, Altaany Z, Yang G, Marazioti A, Zhou Z, et al. Hydrogen sulfide is an endogenous stimulator of angiogenesis. Proc Natl Acad Sci 2009;106(51):21972–7.

[26] Szabo C, Coletta C, Chao C, Módis K, Szczesny B, Papapetropoulos A, et al. Tumor-derived hydrogen sulfide, produced by cystathionine-β-synthase, stimulates bioenergetics, cell proliferation, and angiogenesis in colon cancer. PNAS 2013;110:12474–9.

[27] Wu YC, Wang XJ, Yu Le, Chan FKL, Cheng ASL, Yu J, et al. Hydrogen Sulfide Lowers Proliferation and Induces Protective Autophagy in Colon Epithelial Cells. PLoS ONE 2012;7(5):e37572. doi: https://doi.org/10.1371/journal.pone.0037572.

[28] Wang R, Gu X, Li Q, Gao J, Shi B, Xu Ge, et al. Aggregation Enhanced Responsiveness of Rationally Designed Probes to Hydrogen Sulfide for Targeted Cancer Imaging. J Am Chem Soc 2020;142(35):15084–90.

[29] Xiang J, Xing P, Liu X, Shen P, Shao S, Zhou Q, et al. Hydrogen sulfide-activatable prodrug-backboned block copolymer micelles for delivery of chemotherapeutics. Polym Chem 2021;12(29):4167–74.

[30] Li Y, Chen W, Qi Y, Wang S, Li L, Li W, et al. H2S-Scavenged and Activated Iron Oxide-Hydroxide Nanospindles for MRI-Guided Photothermal Therapy and Ferroptosis in Colon Cancer. Small 2020;16(37):2001356. doi: https://doi.org/10.1002/smll.202001356.

[31] Feng J, Ren W-X, Kong F, Dong Y-B. A covalent organic framework-based nanoagent for H2S-activable phototherapy against colon cancer. Chem Commun 2021;57(59):7240–3.

[32] Ma Yu, Li X, Li A, Yang P, Zhang C, Tang Bo. Xiangyuan Li, Aijie Li, Peng Yang, Caiyun Zhang, Bo Tang, H2S-Activable MOF Nanoparticle Photosensitizer for Effective Photodynamic Therapy against Cancer with Controllable Singlet-Oxygen Release. Angew Chem Int Ed 2017;56(44):13752–6.

[33] Shi B, Yan Q, Tang J, Xin K, Zhang J, Zhu Y, et al. Hydrogen sulfide-activatable second near-infrared fluorescent nanoassemblies for targeted phototherapy cancer therapy. Nano Lett 2018;18(10):6411–6.

[34] Lu K, He C, Guo N, Chan C, Ni K, Weichselbaum RR, et al. Chlorin-Based Nanoscale Metal-Organic Framework Systemically Rejects Colorectal Cancers via Synergistic Photodynamic Therapy and Checkpoint Blockade Immunotherapy. J Am Chem Soc 2016;138(38):12502–10.

[35] Zhu J, Zhang M, Zheng D, Hong S, Feng J, Zhang X-Z. A Universal Approach to Render Nanomedicine with Biological Identity Derived from Cell Membranes. Biomacromolecules 2018;19(6):2043–52.

[36] An Lu, Cao M, Zhang X, Lin J, Tian Q, Yang S. pH and Glutathione Synergistically Triggered Release and Self-Assembly of Au Nanospheres for Tumor Theranostics. ACS Appl Mater Interfaces 2020;12(7):8050–61.

[37] Chen M-M, Hao H-L, Zhao W, Zhao X, Chen H-Y, Xu J-J. A plasmon-enhanced theranostic nanoplatform for synergistic chemo-phototherapy of hypoxic tumors in the NIR-II window. Chem Sci 2021;12(32):10848–54.

[38] Zhang Y, Wang L, Liu L, Lin L, Liu F, Xie Z, et al. Engineering Metal-Organic Frameworks for Photoacoustic Imaging-Guided Chemo-/Photothermal Combinational Tumor Therapy. ACS Appl Mater Interfaces 2018;10 (48):41035–45.

[39] Wang X-G, Cheng Q, Yu Y, Zhang X-Z. Controlled Nucleation and Controlled Growth for Size Predicable Synthesis of Nanoscale Metal-Organic Frameworks (MOFs): A General and Scalable Approach. Angew Chem Int Ed 2018;57 (26):7836–40.

[40] Sun Q, Sheng J, Yang R. Encapsulation of curcumin in CD-MOFs: promoting its incorporation into water-based products and consumption. Food Funct 2021;12(21):10795–805.

[41] Mei L, Zhang X, Yin W, Dong X, Guo Z, Fu W, et al. Translocation, biotransformation-related degradation, and toxicity assessment of polyvinylpyrrolidone-modified 2H-phase nano-MoS2. Nanoscale 2019;11 (11):4767–80.

[42] Marković ZM, Kepić DP, Matijašević DM, Pavlović VB, Jovanović SP, Stanković NK, et al. Todorović Marković, Ambient light induced antibacterial action of curcumin/graphene nanomesh hybrids. RSC Adv 2017;7(57):36081–92.

[43] van der Zee J. Heating the patient: a promising approach? Ann Oncol 2002;13 (8):1173–84.